Supplementary Information for: Blood osmolytes such as sugar can drive brain fluid flows in a poroelastic model Scientific Reports

Peter Bork, Michael Gianetto, Evan Newbold, Lauren Hablitz, Tomas Bohr, and Maiken Nedergaard

2024

Contents

1 Pressure and fluid flow within the tissue domain

We start from mass-conservation of the brain fluid[1] with density ρ in pores with volume fraction ϕ and velocity $\boldsymbol{v}$,

$$\frac{\partial(\rho\phi)}{\partial t} + \nabla\cdot(\rho\phi\boldsymbol{v}) = \tilde{q}. \tag{1}$$

Here, $\tilde{q}$ is a source/sink term corresponding to fluid production or absorption across a small fraction of the pore wall, the blood-brain barrier. We will restrict our main analyses to steady states and additionally assume constant porosity and fluid density. This gives

$$\nabla\cdot\boldsymbol{v} = \frac{\tilde{q}}{\rho\phi} = q, \tag{2}$$

where q is now a production rate of brain fluid (in units of per time).[2]

The production across the blood brain barrier is given by the Kedem-Katchalsky equations, though we disregard solute transfer and have the rate

$$q = -\tilde{A}_b L_P(P-\Psi). \tag{3}$$

Here, $\tilde{A}_b$ is the area of blood brain barrier in a unit volume of brain tissue, L_p is the specific hydraulic permeability, P is the interstitial fluid pressure and Ψ is the water potential of the capillaries. The water potential with a standard definition using van 't Hoff's relation is

$$\Psi \equiv p_b - RT\Delta c, \tag{4}$$

where p_b is average blood pressure in the given infinitesimal volume section, R is the gas constant T is the temperature, and $\Delta c = c_c - c$ is the osmolyte concentration difference between capillaries (c_c) and interstitial fluid (c, both number densities).

Darcy's law relates the fluid pressure and its velocity in the tissue pores,

$$\nabla p = -\frac{\eta}{\kappa}\boldsymbol{v}, \tag{5}$$

where κ is the tissue permeability and η the viscosity of the interstitial fluid. The tissue permeability is related to the cross-sectional area of pores and pore throats. Since the extracellular space has much larger pores, we can ignore the aquaporins and intracellular spaces for the purposes of applying Darcy's law, and κ should be similar to cross-sectional area of extracellular and perivascular spaces (see for example Nicholson's sheets and tunnels paper [16]).

Taking the divergence of the pressure gradient and combining (3) and (5) gives.

$$\begin{aligned}\Delta p \equiv \nabla\cdot(\nabla p) = \nabla\cdot\left(-\frac{\eta}{\kappa}\boldsymbol{v}\right) = -\frac{\eta}{\kappa}\nabla\cdot\boldsymbol{v}\\ \implies \Delta p = \frac{\eta}{\kappa}\tilde{A}_b L_P(p-\Psi).\end{aligned} \tag{6}$$

We here assumed constant permeability κ and viscosity η. The intrinsic permeability κ depends on the pore structure, which changes due to deformation. However, this effect is second order in the deformation [1] and we can neglect it here.

It is convenient to define the new pressure $P \equiv p - \Psi$, because when the water potential of the blood Ψ is constant or harmonic, we have a proper homogeneous screened Poisson equation with parameter

$$\gamma^2 \equiv \frac{\eta}{\kappa}\tilde{A}_b L_p, \tag{7}$$

namely

$$\Delta P - \gamma^2 P = 0. \tag{8}$$

[1] Meaning any fluid in the brain except blood.

[2] Notice that during compression (when $\frac{\partial\phi}{\partial t} \neq 0$), shrinkage of the tissue implies a fluid flux either across the blood-brain barrier or within the tissue in order to conserve mass, which in this case is mostly water. The magnitude is on the order of the compressed volume divided by the time it takes to complete the compression and will be neglected here.

1.1 Total absorption rate

By integrating the absorption rate q over the domain we get the total volume absorption rate Q,

$$Q = \int_\Omega q \,\mathrm{dV} = -\tilde{\mathrm{A}}_\mathrm{b}\mathrm{L}_\mathrm{p} \int_\Omega (\mathrm{p} - \Psi)\,\mathrm{dV}. \tag{9}$$

This can be compared with values such as cerebrospinal fluid production rate for the whole brain, or estimates of influx to particular brain domains.

2 Biot consolidation

We start from Biot's analysis [3]. Like Biot, we take the strain to be small and have Cauchy's strain tensor components

$$u_{ij} = \tfrac{1}{2}(\nabla_i u_j + \nabla_j u_i), \tag{10}$$

Here, $u_i(x_i) = x_i - X_i(x_i)$ is displacement along axis i in Eulerian frame from the reference position $X(x)$ of the material now at x. Biot arrives at solid phase stresses σ_{ij} as functions of strain

$$\sigma_{ij} = 2\mu u_{ij} + \lambda\delta_{ij}\sum_k u_{kk} - \alpha\delta_{ij}p. \tag{11}$$

We take the Biot parameter $\alpha = 1$ corresponding to incompressible solid and fluid phases. As Biot writes in this case '... the volume change of the soil [here tissue] is equal to the amount of water squeezed out' [3]. Though cell volumes may change, the solid phase here is rather the proteins and fatty acids which are not compressed [6]. This equation (11) is our modified 'Hooke's law' but with an added $\delta_{ij}p$. Mechanical equilibrium (without further body forces) requires

$$\sum_j \nabla_j \sigma_{ij} = 0. \tag{12}$$

Inserting our modified Hooke's law results in

$$\mu\sum_j \nabla_j^2 u_i + (\lambda+\mu)\nabla_i \sum_j \nabla_j u_j - \nabla p = 0 \tag{13a}$$

$$\mu\nabla^2\boldsymbol{u} + (\lambda+\mu)\nabla\nabla\cdot\boldsymbol{u} - \nabla p = \boldsymbol{0}. \tag{13b}$$

Where we use the displacement vector

$$\boldsymbol{u} \equiv u_x\hat{\boldsymbol{e}}_x + u_y\hat{\boldsymbol{e}}_y + u_z\hat{\boldsymbol{e}}_z = \boldsymbol{x} - \boldsymbol{X}(\boldsymbol{x}) \tag{14}$$

to use vector notation with reference position $\boldsymbol{X}(\boldsymbol{x})$ for the material now at $\boldsymbol{x}$. Equations (13) are the Navier-Cauchy equation but with body force equal to the divergence of the pore pressure. This result is given as equation (19) in Macminn et al. [14], and is the one-network equivalent of Tully and Ventikos' model [19].

2.0.1 Convenient relationships between elastic moduli

For reference, some useful relationships between elastic moduli.

$$E = \mu\frac{3\lambda+2\mu}{\lambda+\mu}, \qquad \nu = \frac{\lambda}{2(\lambda+\mu)}, \tag{15a}$$

$$\lambda = \frac{E\nu}{(1-2\nu)(1+\nu)}, \qquad \mu = \frac{E}{2(1+\nu)}, \tag{15b}$$

$$M \equiv 2\mu + \lambda. \tag{15c}$$

3 Spherical brain geometry

3.1 Pressure and flow

The homogeneous screened Poisson equation (8) in spherical coordinates with spherical symmetry is

$$r^{-2}\frac{\partial}{\partial r}\left(r^2\frac{\partial}{\partial r}P(r)\right)-\gamma^2 P(r)=0. \tag{16}$$

Our model brain is an annular sphere with inner radius a (corresponding to the ventricle radius) and outer radius b (corresponding to the subarachnoid space). With Dirichlet boundaries where $r=a$ and $r=b$ we have a well-defined problem with

$$P_a=p(a)-\Psi \qquad P_b=p(b)-\Psi. \tag{17}$$

The solution is

$$p(r)=\frac{aP_a\left[e^{\gamma(a-2b+r)}-e^{\gamma(a-r)}\right]+bP_b\left[e^{\gamma(2a-b-r)}-e^{-\gamma(b-r)}\right]}{\left[e^{2\gamma(a-b)}-1\right]r}+\Psi \tag{18}$$

The once- and twice-differentiated pressure will be useful,

$$p'(r)=\frac{aP_a\left[(\gamma r-1)e^{\gamma(a-2b+r)}+(\gamma r+1)e^{\gamma(a-r)}\right]-bP_b\left[(\gamma r+1)e^{\gamma(2a-b-r)}+(\gamma r-1)e^{-\gamma(b-r)}\right]}{\left[e^{2\gamma(a-b)}-1\right]r^2} \tag{19a}$$

$$\begin{aligned}p''(r)=&\frac{aP_a\left[(\gamma^2r^2-2\gamma r+2)e^{\gamma(a-2b+r)}-(\gamma^2r^2+2\gamma r+2)e^{\gamma(a-r)}\right]}{\left[e^{2\gamma(a-b)}-1\right]r^3}\\&+\frac{bP_b\left[(\gamma^2r^2+2\gamma r+2)e^{\gamma(2a-b-r)}-(\gamma^2r^2-2\gamma r+2)e^{-\gamma(b-r)}\right]}{\left[e^{2\gamma(a-b)}-1\right]r^3}.\end{aligned} \tag{19b}$$

We specifically measure pressure relative to cerebrospinal fluid pressure and take the pressures in ventricles and subarachnoid spaces to be equal,

$$p(a)=p(b)=0 \implies P(a)=P(b)=-\Psi. \tag{20}$$

The solution is then

$$p(r)=\Psi\left(1-\frac{a\left[e^{\gamma(a-2b+r)}-e^{\gamma(a-r)}\right]+b\left[e^{\gamma(2a-b-r)}-e^{-\gamma(b-r)}\right]}{\left[e^{2\gamma(a-b)}-1\right]r}\right). \tag{21}$$

Total filtration rate. For the symmetrical sphere, the integral in equation (9) becomes

$$Q=4\pi\tilde{A}_bL_p\int_a^b r^2(p-\Psi)\mathrm{d}r \tag{22a}$$

$$=4\pi\frac{\tilde{A}_bL_p}{\gamma^2}\left[\frac{(aP_a-\gamma a^2P_a-\gamma b^2P_b-bP_b)e^{2\gamma(a-b)}+2\gamma ab(P_a+P_b)e^{\gamma(a-b)}-a(a\gamma+1)P_a-b(b\gamma-1)P_b}{e^{2\gamma(a-b)}-1}\right] \tag{22b}$$

For $P_a=P_b=-\Psi$ we get

$$Q=4\pi\Psi\kappa\frac{(b-a)\sinh(\gamma(b-a))-\gamma(a^2+b^2)\cosh(\gamma(b-a))+2\gamma ab}{\eta\sinh(\gamma(b-a))} \tag{22c}$$

Notice that by definition

$$\frac{\tilde{A}_bL_p}{\gamma^2}=\frac{\kappa}{\eta}.$$

3.2 Compression

This section follows Lautrup [12] pp. 153-154, but with an added pressure term as described above. In spherical coordinates with spherical symmetry where $\boldsymbol{u} = u_r \hat{\boldsymbol{e}}_r$ and $\nabla p = p' \hat{\boldsymbol{e}}_r$, we have $\nabla\nabla \cdot \boldsymbol{u} = \nabla^2 \boldsymbol{u}$ and the Navier-Cauchy equation (13) takes the form

$$M \nabla\nabla \cdot \boldsymbol{u} = \nabla p. \tag{23}$$

This gives an ODE for the radial component u_r

$$M \frac{\mathrm{d}}{\mathrm{d}r} \left(\frac{1}{r^2} \frac{\mathrm{d}(r^2 u_r)}{\mathrm{d}r} \right) = p' \tag{24}$$

The general solution using equation (16) is

$$u_r = C_1 r + \frac{C_2}{r^2} + \gamma^{-2} M^{-1} p', \tag{25}$$

where C_1 and C_2 are integration constants. The strain tensor in this case is symmetric and equal to the gradient of the displacement field, $\nabla \boldsymbol{u} = \mathbf{u}$. The non-vanishing components of the strain tensor are therefore

$$u_{rr} = u_r' \qquad u_{tt} = \frac{u_r}{r}. \tag{26}$$

From equation (11), the radial component of the stress tensor is

$$\begin{aligned} \sigma_{rr} &= M u_r' + 2\lambda \frac{u_r}{r} - p \\ &= M(C_1 - \frac{2C_2}{r^3} + \gamma^{-2} M^{-1} p'') + 2\lambda \left(C_1 + \frac{C_2}{r^3} + \frac{p'}{M\gamma^2 r} \right) - p. \end{aligned} \tag{27}$$

The boundary conditions are that the inner surface is free, $\sigma_{rr}(a) = 0$, and the outer surface is fixed, $u_r(b) = 0$. The free boundary gives the condition

$$\sigma_{rr}(a) = 0 = M u_r'(a) + 2\lambda \frac{u_r(a)}{a} - p(a) \tag{28}$$

$$\implies 0 = 3KC_1 - 4a^{-3}\mu C_2 + D_1, \tag{29}$$

$$D_1 \equiv \gamma^{-2} p''(a) + \frac{2\nu}{(1-\nu)\gamma^2 a} p'(a) - p(a) \tag{30}$$

Notice that $(3\lambda + 2\mu) = 3K$ where K is the bulk modulus, and $\lambda/M = \nu/(1-\nu)$ where ν is Poisson's ratio. The fixed end gives the condition

$$\begin{aligned} u_r(b) = 0 &= bC_1 + b^{-2} C_2 + D_2 \\ D_2 &\equiv \gamma^{-2} M^{-1} p_b' \end{aligned} \tag{31}$$

Solving these two equations for the two constants give

$$C_1 = -\frac{1}{d} \left(4\mu a^{-3} D_2 + b^{-2} D_1 \right) = -\frac{1}{d} \left(\frac{2E}{1+\nu} a^{-3} D_2 + b^{-2} D_1 \right) \tag{32a}$$

$$C_2 = \frac{1}{d}(bD_1 - 3KD_2) \tag{32b}$$

$$d \equiv 3b^{-2}K + 4a^{-3}\mu b = 3b^{-2}K + 2ba^{-3}\frac{E}{1+\nu} \tag{32c}$$

For the special case of $p_a = p_b = 0$,

$$C_1 = \frac{4\Psi}{(1-e^{-\gamma(b-a)})a^3\gamma^2}\left((\gamma a-1)(\mu\gamma^4a^2-\frac{1}{2})(e^{-\gamma(b-a)}(1-e^{2\gamma a})+ae^{2\gamma a})\right. \tag{33}$$

$$\left.+[(\mu\gamma^4+\tfrac{1}{4}\gamma^2)a^3-\mu\gamma^5a^4+\tfrac{1}{2}a^2\gamma-\tfrac{1}{2}a]e^{-2\gamma(b-a)}-\frac{\gamma^2a^3}{4}\right) \tag{34}$$

$$C_2 = \frac{\Psi}{\gamma^2 M}\frac{(1-\gamma b)[ae^{\gamma(a-b)}-ae^{\gamma(a+b)}+b(e^{2\gamma a}-1)]}{(1-e^{-2\gamma(b-a)})b^2}. \tag{35}$$

Estimate of boundary stress With the estimates given below, we arrive at a stress at the outer boundary ($b = 10^{-3}$m) of $\sigma_{rr}(b) = 82\,\mathrm{Pa}$. This is less than 10% of our estimate of Young's modulus and we find it reasonable that the anatomical structures can sustain this stress.

Volume compression We calculate the volume of the tissue with

$$V = \frac{4}{3}\pi([b+u_r(b)]^3-[a+u_r(a)]^3), \tag{36}$$

and the relative volume compression is therefore $(V-V_0)/V_0$ where V_0 is the volume without deformation, $u_r = 0$.

4 Net filtration

When blood water potential is lowered (such as following hydration), the model predicts net filtration, or production or interstitial fluid from vasculature, see Figure 1 and discussion in the main text.

5 Parameter estimates

Screening length γ^{-1}. To set the central parameter

$$\gamma^2 = \frac{\eta}{\kappa}\tilde{A}_bL_p, \tag{37}$$

we start in order of appearance. The viscosity has a standard value, $\eta \approx 1.5\times10^{-3}\mathrm{Pa\,s}$.

The permeabiltiy κ has a range of values. Based on post-mortem sections of microscopic tissue, Holter et al. (2017) estimate $\kappa = 10^{-17}\mathrm{m}^2$ [9]. Basser (1992) uses a deformation model of pressure-infusion into the brain based on Biot's consolidation and in general very similar to ours, fits *in-vivo* data to this model, and estimates an effective permeability of $\kappa = 5\times10^{-14}\,\mathrm{m}^2$ [2][3]. More recently, Støverud and colleagues modelling of pressure-infusion to brain tumours fit the data best with $\kappa = 1.82\times10^{-15}\,\mathrm{m}^2$.

The relative blood brain barrier area can be estimated from blood volume fraction and vessel radii. The microvessels occupy roughly 2% of the tissue volume [20] with mean radii at $\bar{r}_b = 2\mu\mathrm{m}$ [4]. When $\tilde{l}_b$ is the length of microvessels in a unit tissue volume, then

$$\pi r_b^2\tilde{l}_b = 2\% \implies \tilde{l}_b = \frac{2}{100\pi r_b^2}. \tag{38a}$$

The relative area of blood brain barrier is the corresponding circumference

$$\tilde{A} = 2\pi r_b\tilde{l}_b = 2\pi r_b\times\frac{2}{100\pi r_b^2} = \frac{4}{100r_b}. \tag{38b}$$

[3]Basser gives $\kappa = 5\times10^{-9}$ in units $\mathrm{cm}^4/\mathrm{dynes\text{-}sec}$ for gray matter and corresponding $\kappa = 7.5$ for white matter. We use grey matter and convert with dyne = 0.1 Pa cm^2.

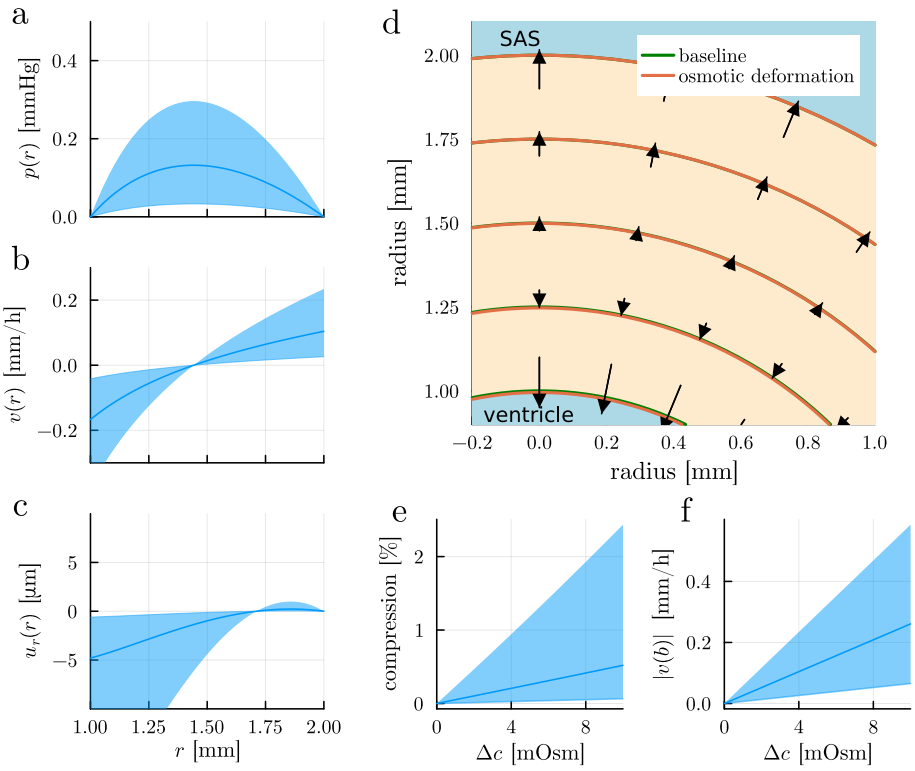

Figure 1: Model simulation of hypotonic blood. With blood hypotonicity corresponding to an osmolyte concentration difference of 3mM across blood brain barrier, the model predicts net efflux of fluid from brain to cerebrospinal fluid. a) pressure, b) velocity, c) displacement, all over the radial axis (in c). d) The deformation is very small in this case, but the interstitial velocity reaches nearly 1mm/h (black arrows). e) Compression and f) superficial velocity as functions of osmolyte concentration difference.

Parameter	value	description	ref.
η	$10^{-3}\,\mathrm{Pa\,s}$	viscosity	Bloomfield 1998 [5]
κ	$1.8\times10^{-15}\,\mathrm{m}^2$	permeability	Støverud 2012 [18]
L_p	$5\times10^{-12}\,\mathrm{m\,Pa^{-1}\,s^{-1}}$	arteriolar permeability	Michel 1999 [15]
$\tilde{A}_b$	$5\times10^{3}\,\mathrm{m^{-1}}$	relative BBB area	Own estimate.
E	1 kPa	Young's modulus (young sleeping brain)	Ge 2022 [7]
ν	0.4	Poisson's ratio	Støverud 2012 [18]
R	$8314\mathrm{L\,Pa\,K^{-1}\,mol^{-1}}$	gas constant, equals in $\mathrm{Pa\,K^{-1}M^{-1}}$.	-
T	300K	brain temperature	-
Ψ	-120kPa	Osmotic pressure imbalance	Own estimate.
γ^{-1}	8.5 mm	Screening length	Own estimate.

Table 1: Parameters.

With $r_b \approx 2\times10^{-6}\,\mathrm{m}$, $\tilde{A} = \frac{1}{2}\times10^{4}\mathrm{m}^{-1} = 5\times10^{3}\mathrm{m}^{-1}$.

Kimura et al. (1993)[10] provide a median estimate of isolated arterioles from rat cortex hydraulic permeability at $L_p \approx 6\times10^{-10}\,\mathrm{m\,Pa^{-1}\,s^{-1}}$. This is in the same order of magnitude as a recent estimate of endfoot sheath permeability [11], and therefore perhaps too high. The perhaps authoritative review is Michel and Curry (1999) [15] in which (non-fenestrated) hind-limb microvessels are reported to have hydraulic permeability $L_p \in [1,5]\times10^{-12}\,\mathrm{m\,Pa^{-1}\,s^{-1}}$. On balance, the estimates by Michel are likely better than Kimura, in light also of the endfoot estimates, but we choose the upper end from Michel since Kimura is afterall based on brain vessels.

The product γ^2 is therefore

$$\gamma^2 \equiv \frac{\eta}{\kappa}\tilde{A}_b L_p \tag{39a}$$

$$\approx 13889\mathrm{m}^{-2}, \tag{39b}$$

$$\implies \gamma \approx 118\,\mathrm{m}^{-1}, \tag{39c}$$

$$\implies \gamma^{-1} = 8.5\,\mathrm{mm}. \tag{39d}$$

Stiffness E and Poisson's ratio ν. The most recent and advanced methods for determining brain elasticity uses a technique called optical coherence tomography reverberant shear wave elastography [7]. These authors find the Young's modulus to increase from 8kPa to 15kPa for the sleeping brain exposed to waves of from 1Hz to 3kHz, while their estimate of the equlibrium value is 1kPa (figure 8, table 1). A more traditional estimate is that due to magnetic resonance elastography at 90Hz by Green et al., where Young's modulus estimate is 2.65kPa [8]. Since our dynamics are slower by some orders of magnitude, we are forced to speculate, and choose $E = 1\,\mathrm{kPa}$. We take Poisson's ratio to be $\nu = 0.4$, as argued best fits infusion data by Støverud et al. 2012 [18].

Water potential imbalance Ψ. The average osmotic imbalance Ψ averaged over small tissue volumes which include arterioles, capillaries and venules will be weighted by surface area and therefore dominated by the capillary component. Mayhan and Heistad (1986) reports arteriolar pressures of 59 ± 5mmHg with venular pressures at 7 ± 1mmHg (mean $\pm$ SE). Since the pressure drops linearly along the capillaries, we take the simple average of these two values to get a mean blood pressure of $p_b = 33$mmHg$= 4390$Pa. Assuming osmolytes are balanced at baseline, and elevated by $\Delta c = 50$mOsm reported by [17, 13], the osmotic imbalance is

$$\Psi = p_b - RT\Delta c = 4390 - 8314\times300\times0.05 = -120\,\mathrm{kPa}. \tag{40}$$

References

[1] L. C. Auton and C. W. MacMinn, *From arteries to boreholes: steady-state response of a poroelastic cylinder to fluid injection*, Proceedings of the Royal Society A: Mathematical, Physical and Engineering Sciences, 473 (2017), p. 20160753.

[2] P. J. Basser, *Interstitial pressure, volume, and flow during infusion into brain tissue*, Microvascular research, 44 (1992), pp. 143–165.

[3] M. A. Biot, *General theory of three-dimensional consolidation*, Journal of applied physics, 12 (1941), pp. 155–164.

[4] P. Blinder, P. S. Tsai, J. P. Kaufhold, P. M. Knutsen, H. Suhl, and D. Kleinfeld, *The cortical angiome: an interconnected vascular network with noncolumnar patterns of blood flow*, Nature neuroscience, 16 (2013), pp. 889–897.

[5] I. Bloomfield, I. Johnston, and L. Bilston, *Effects of proteins, blood cells and glucose on the viscosity of cerebrospinal fluid*, Pediatric neurosurgery, 28 (1998), pp. 246–251.

[6] C. Cadart, L. Venkova, P. Recho, M. C. Lagomarsino, and M. Piel, *The physics of cell-size regulation across timescales*, Nature Physics, 15 (2019), pp. 993–1004.

[7] R. G. Ge, W. Song, M. Nedergaard, J. P. Rolland, and K. J. Parker, *Theory of sleep/wake cycles affecting brain elastography*, Physics in Medicine & Biology, 67 (2022), p. 225013.

[8] M. A. Green, L. E. Bilston, and R. Sinkus, *In vivo brain viscoelastic properties measured by magnetic resonance elastography*, NMR in Biomedicine: An International Journal Devoted to the Development and Application of Magnetic Resonance In vivo, 21 (2008), pp. 755–764.

[9] K. E. Holter, B. Kehlet, A. Devor, T. J. Sejnowski, A. M. Dale, S. W. Omholt, O. P. Ottersen, E. A. Nagelhus, K.-A. Mardal, and K. H. Pettersen, *Interstitial solute transport in 3d reconstructed neuropil occurs by diffusion rather than bulk flow*, Proceedings of the National Academy of Sciences, 114 (2017), pp. 9894–9899.

[10] M. Kimura, H. H. Dietrich, V. H. Huxley, D. R. Reichner, and R. G. Dacey Jr, *Measurement of hydraulic conductivity in isolated arterioles of rat brain cortex*, American Journal of Physiology-Heart and Circulatory Physiology, 264 (1993), pp. H1788–H1797.

[11] T. Koch, V. Vinje, and K.-A. Mardal, *Estimates of the permeability of extra-cellular pathways through the astrocyte endfoot sheath*, Fluids and Barriers of the CNS, 20 (2023), pp. 1–18.

[12] B. Lautrup, *Physics of continuous matter: exotic and everyday phenomena in the macroscopic world*, CRC press, 2011.

[13] T. O. Lilius, M. Rosenholm, L. Klinger, K. N. Mortensen, B. Sigurdsson, F. L.-H. Mogensen, N. L. Hauglund, M. S. N. Nielsen, T. Rantamäki, and M. Nedergaard, *Spect/ct imaging reveals cns-wide modulation of glymphatic cerebrospinal fluid flow by systemic hypertonic saline*, Iscience, 25 (2022).

[14] C. W. MacMinn, E. R. Dufresne, and J. S. Wettlaufer, *Large deformations of a soft porous material*, Physical Review Applied, 5 (2016), p. 044020.

[15] C. Michel and F. Curry, *Microvascular permeability*, Physiological reviews, (1999).

[16] C. Nicholson, *Sheet and void porous media models for brain interstitial space*, Journal of the Royal Society Interface, 20 (2023), p. 20230223.

[17] B. A. Plog, H. Mestre, G. E. Olveda, A. M. Sweeney, H. M. Kenney, A. Cove, K. Y. Dholakia, J. Tithof, T. D. Nevins, I. Lundgaard, et al., *Transcranial optical imaging reveals a pathway for optimizing the delivery of immunotherapeutics to the brain*, JCI insight, 3 (2018).

[18] K. H. Støverud, M. Darcis, R. Helmig, and S. M. Hassanizadeh, *Modeling concentration distribution and deformation during convection-enhanced drug delivery into brain tissue*, Transport in porous media, 92 (2012), pp. 119–143.

[19] B. Tully and Y. Ventikos, *Cerebral water transport using multiple-network poroelastic theory: application to normal pressure hydrocephalus*, Journal of Fluid Mechanics, 667 (2011), pp. 188–215.

[20] P. Vérant, R. Serduc, B. Van Der Sanden, C. Rémy, and J.-C. Vial, *A direct method for measuring mouse capillary cortical blood volume using multiphoton laser scanning microscopy*, Journal of Cerebral Blood Flow & Metabolism, 27 (2007), pp. 1072–1081.